

## Secondary quasiperiodicity in the peroxidase–oxidase reaction

Lars F. Olsen,<sup>\*a</sup> Tatiana V. Bronnikova<sup>b</sup> and William M. Schaffer<sup>b</sup>

<sup>a</sup> CELCOM, Department of Biochemistry and Molecular Biology, SDU Odense University, Campusvej 55, DK-5230 Odense M, Denmark. E-mail: lfo@dou.dk

<sup>b</sup> Department of Ecology and Evolutionary Biology, University of Arizona, Tucson, Arizona 85721, USA

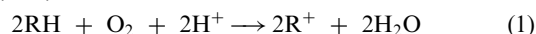
Received 14th August 2001, Accepted 27th September 2001

First published as an Advance Article on the web 6th December 2001

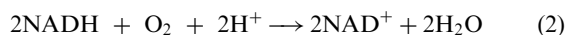
Secondary quasiperiodicity (period-doubled oscillations modulated by an incommensurate frequency), or “Q2”, is the temporal manifestation of quasiperiodic motion on period-doubled tori. The existence of this regime in a chemical reaction was first predicted (T. V. Bronnikova, W. M. Schaffer and L. F. Olsen, *J. Chem. Phys.*, 1996, **105**, 10 849) in the course of numerical explorations of a detailed model of the peroxidase–oxidase system. Subsequent analysis (T. V. Bronnikova, W. M. Schaffer, M. J. B. Hauser and L. F. Olsen, *J. Phys. Chem. B*, 1998, **102**, 632) suggested the possibility of homoclinic transitions (“fat torus” bifurcation) to chaos involving Q2. In the present paper, we present the first experimental evidence for secondary quasiperiodicity and fat torus bifurcations in a chemical oscillator. We also identify a second (“thin torus”) route to chaos involving Q2. The relationship of these two bifurcation scenarios to each other and to the experimental findings is discussed.

### 1. Introduction

The oscillating peroxidase–oxidase (PO) reaction<sup>1–4</sup> is a series of reactions, or elementary steps (Table 1), whereby an organic electron donor, RH, is oxidized by molecular oxygen in the presence of peroxidase enzyme to yield oxidized electron donor and water, *i.e.*,



Over the years, the PO reaction has become a model system for the experimental investigation of nonlinear biochemical dynamics, in which capacity it is arguably the biochemical counterpart of the celebrated Belousov–Zhabotinskii reaction.<sup>5,6</sup> The most widely studied version of reaction (1) utilizes NADH as the electron donor and horseradish peroxidase (HRP) as the catalyzing enzyme. In this case, the balance equation becomes



In the presence of Methylene Blue (MB) and an aromatic cofactor such as 2,4-dichlorophenol (DCP), and with continuing inputs of NADH and O<sub>2</sub>, reaction (2) can oscillate. Both simple<sup>1,2</sup> and complex<sup>7</sup> cycles have been observed along with quasiperiodicity<sup>7,8</sup> and chaos.<sup>9</sup>

In previous papers,<sup>10,11</sup> we reported on the consequences of increasing the average NADH concentration, [NADH]<sub>av</sub>, by adjusting that compound’s flow rate into the reactor. These experiments established that the response to varying [NADH]<sub>av</sub> is pH-dependent. For pH values ≤ 5.2, period-doubling transitions to chaos are observed. At higher pH values (up to 6.3), period-adding transitions are obtained under otherwise similar conditions. In both cases, continuing increases in [NADH]<sub>av</sub> result in reverse period-doublings leading to a steady state. In short, the overall dynamical picture is one of period-bubbling<sup>12</sup> complicated by additional bifurcations at intermediate values of the control parameter.

The concentration of aromatic cofactor can also be used as a bifurcation parameter. For instance, increasing the concentration of DCP at pH 5.1<sup>13</sup> results in a period-doubling route to chaos similar to what one observes when [NADH]<sub>av</sub>

is varied at pH 5.2. In the present paper, we substitute 4-hydroxybenzoic acid (HBA) for DCP and study the bifurcations which result when [HBA] is varied for fixed values of [NADH]<sub>av</sub>. These experiments were performed at both low ( $4.7 \times 10^{-3} \text{ s}^{-1}$ ) and high ( $5.7 \times 10^{-3} \text{ s}^{-1}$ ) values of the oxygen transfer constant. In both cases, the pH was 6.3.

A detailed model implementing the elementary steps in Table 1 was first proposed<sup>14</sup> in 1995. This scheme, which we call BFSO, gives semi-quantitative agreement with the principal experimental results reported to date.<sup>11,14–17</sup> BFSO also predicts the existence of dynamical states not yet observed experimentally. These include quasiperiodic motion on period-doubled tori.<sup>15,18</sup> An example of this state, also called secondary quasiperiodicity (Q2),<sup>18</sup> is shown in Fig. 1. When viewed in the time domain (Fig. 1), reactant concentrations evidence period-doubled cycles modulated by an incommensurate frequency. Poincaré sections (Fig. 2b) of phase portrait *projections* onto [O<sub>2</sub>]-[NAD]-[NADH] space (Fig. 2a) reflect the underlying toroidal topology. By way of contrast, Poincaré sections (Fig. 2d) of phase portrait *reconstructions* (Fig. 2c) obtained by embedding<sup>19</sup> univariate time series are ambiguous. This is because the reconstructed attractors are highly compressed and the associated Poincaré sections effectively indistinguishable from a curve. In this case, the toroidal nature of the flow is established by imagining that the sections are, in fact, one-dimensional and computing return maps (Fig. 2e) in the manner described, for example, by Roux *et al.*<sup>20</sup>

In this paper, we present experimental evidence for secondary quasiperiodicity in reaction (2). So far as we are aware, these data constitute the first observation of Q2 in a chemical reaction. We further observe that the BFSO model predicts the existence of secondary quasiperiodicity for parameter values concordant with the experimental conditions under which this state is observed. There is, however, a discrepancy. In the simulation shown in Fig. 2, the system is close to a “fat torus”<sup>15</sup> bifurcation whereby the loops of a period doubled torus interact with each other and with the stable manifold of the non-stable period-one cycle which lies between them. The experimentally observed double torus on which we report here

**Table 1** Selected elementary steps of the PO reaction and rate constants used in simulation

Reaction	Rate equation	Rate constant/Flux
1. $\text{NADH} + \text{O}_2 + \text{H}^+ \xrightarrow{k_1} \text{NAD}^+ + \text{H}_2\text{O}_2$	$k_1[\text{NADH}][\text{O}_2]$	$3.0 \text{ M}^{-1} \text{ s}^{-1}$
2. $\text{H}_2\text{O}_2 + \text{Per}^{3+} \xrightarrow{k_2} \text{coI}$	$k_2[\text{H}_2\text{O}_2][\text{Per}^{3+}]$	$1.8 \times 10^7 \text{ M}^{-1} \text{ s}^{-1}$
3. $\text{coI} + \text{NADH} \xrightarrow{k_3} \text{coII} + \text{NAD}^*$	$k_3[\text{coI}][\text{NADH}]$	$4.0 \times 10^4 \text{ M}^{-1} \text{ s}^{-1}$
4. $\text{coII} + \text{NADH} \xrightarrow{k_4} \text{Per}^{3+} + \text{NAD}^*$	$k_4[\text{coII}][\text{NADH}]$	$2.6 \times 10^4 \text{ M}^{-1} \text{ s}^{-1}$
5. $\text{NAD}^* + \text{O}_2 \xrightarrow{k_5} \text{NAD}^+ + \text{O}_2^-$	$k_5[\text{NAD}^*][\text{O}_2]$	$2.0 \times 10^7 \text{ M}^{-1} \text{ s}^{-1}$
6. $\text{O}_2^- + \text{Per}^{3+} \xrightarrow{k_6} \text{coIII}$	$k_6[\text{O}_2^-][\text{Per}^{3+}]$	$1.7 \times 10^7 \text{ M}^{-1} \text{ s}^{-1}$
7. $2\text{O}_2^- + 2\text{H}^+ \xrightarrow{k_7} \text{H}_2\text{O}_2 + \text{O}_2$	$k_7[\text{O}_2^-]^2$	$5.0 \times 10^6 \text{ M}^{-1} \text{ s}^{-1}$
8. $\text{coIII} + \text{NAD}^* \xrightarrow{k_8} \text{coI} + \text{NAD}^+$	$k_8[\text{coIII}][\text{NAD}^*]$	Variable
9. $2\text{NAD}^* \xrightarrow{k_9} \text{NAD}_2$	$k_9[\text{NAD}^*]^2$	$6.0 \times 10^7 \text{ M}^{-1} \text{ s}^{-1}$
10. $\text{Per}^{3+} + \text{NAD}^* \xrightarrow{k_{10}} \text{Per}^{2+} + \text{NAD}^+$	$k_{10}[\text{Per}^{3+}][\text{NAD}^*]$	$1.8 \times 10^6 \text{ M}^{-1} \text{ s}^{-1}$
11. $\text{Per}^{2+} + \text{O}_2 \xrightarrow{k_{11}} \text{coIII}$	$k_{11}[\text{Per}^{2+}][\text{O}_2]$	$1.0 \times 10^5 \text{ M}^{-1} \text{ s}^{-1}$
12. $\text{NADH}(\text{stock}) \xrightarrow{k_{12}} \text{NADH}$	$k_{12}[\text{NADH}]_{\text{stock}} (= \text{NI})$	Variable
13. $\text{O}_2(\text{gas}) \xrightleftharpoons[k_{-13}]{k_{13}} \text{O}_2(\text{liquid})$	$k_{13}[\text{O}_2]_{\text{eq}} - k_{-13}[\text{O}_2]$	Both constants variable
14. $\text{NADH} + \text{H}^+ + \text{O}_2^- \xrightarrow{k_{14}} \text{NAD}^* + \text{H}_2\text{O}_2$	$k_{14}[\text{NADH}][\text{O}_2^-]$	$3.0 \times 10^2 \text{ M}^{-1} \text{ s}^{-1}$

is also “fat.” So it would appear that we have evidence not only for a novel dynamical state, but also for a heretofore unobserved route to chaos. Interestingly, however, for parameter values appropriate to the present experiments, BFSO predicts the existence of “thin” tori, the inner margins of which are far from overlapping. Numerical explorations suggest that these tori can also undergo homoclinic transitions to chaos, *via* “thin torus” bifurcations which are topologically distinct from the fat torus route discussed above. Moreover, the two routes (fat and thin) can interact in interesting ways.

## 2. Experimental

Experiments were conducted in a semibatch reactor. The reactor was either a quartz cuvette with a liquid volume of 10 mL and an optical path length of 2.2 cm or a plexiglass cuvette with a liquid volume of 7 mL and an optical path length of 1.8 cm. The cuvette is fitted with a thermostating jacket which maintains the temperature at  $28.0 \pm 0.1$  °C throughout the experiment. The set-up which is fitted with an oxygen electrode and is mounted in a Zeiss Specord 10 diode array spectrophotometer has been described previously.<sup>11</sup> The spectrophotometer records a spectrum of the reaction mixture in the interval 350 to 600 nm every 2s and stores it to a file together with the oxygen concentration in the liquid. These data are later used to calculate the concentrations of NADH and the enzyme species ferric peroxidase ( $\text{Per}^{3+}$ ), ferrous peroxidase ( $\text{Per}^{2+}$ ) and compound III (coIII) as described in ref. 21. Two other enzyme intermediates, compound I (coI) and

compound II (coII) could not be resolved from the absorbance data.<sup>21</sup> The reaction mixture consisted of 0.1 mM sodium phosphate, pH 6.3, containing 1.5  $\mu\text{M}$  horseradish peroxidase, 200–500  $\mu\text{M}$  4-hydroxybenzoic acid (HBA) and 0.1  $\mu\text{M}$  Methylene Blue (MB). NADH is supplied to this solution as a 0.1 M aqueous solution from a syringe *via* a precise step-motor driven pump, while oxygen is fed to the reactor from an  $\text{O}_2/\text{N}_2$  gas mixture supplied to an approximately 10 mL gas head space above the liquid. The solution is stirred with a stirrer inserted into the liquid from above. The stirring rate was adjusted to 900–1200 rpm in order to obtain oxygen transfer constants of either  $4.7(\pm 0.1) \times 10^{-3} \text{ s}^{-1}$  (plexiglass cuvette) or  $5.7(\pm 0.2) \times 10^{-3} \text{ s}^{-1}$  (quartz cuvette).

Prior to the start of each experiment, the reaction mixture containing enzyme, MB and HBA in buffer was equilibrated at 28 °C with pure nitrogen. Experiments were typically started by adding NADH at a flow rate of 40–60  $\mu\text{L h}^{-1}$ . As the absorbance at 360 nm reached a level corresponding to 100 ( $\pm 5$ )  $\mu\text{M}$  NADH the content of the gas phase was changed from pure  $\text{N}_2$  to a 1.05% (v/v) mixture of  $\text{O}_2$  and  $\text{N}_2$ . Then the flow rate was adjusted such that the NADH concentration remained constant at 100  $\mu\text{M}$ . This implied flow rates of 53.4 ( $\pm 4.5$ )  $\mu\text{L h}^{-1}$  in the quartz cuvette and 32.4 ( $\pm 3.2$ )  $\mu\text{L h}^{-1}$  in the plexiglass cuvette. A few experiments were made where the NADH concentration is adjusted to another value.

In order to assure that the results obtained in the plexiglass and the quartz cuvette were independent of the material, and hence only dependent on the oxygen transfer constant we performed additional experiments using the same oxygen transfer constants in both set-ups. Within experimental error we obtain the same dynamics in both cuvettes using the same experimental conditions.

Horseradish peroxidase (RZ 3.0) and NADH disodium salt were purchased from Boehringer Mannheim; Methylene Blue was obtained from Merck and 4-hydroxybenzoic acid was kindly supplied from the Department of Chemistry, SDU Odense University.

## 3. Experimental results

### Low oxygen transfer constant experiments

For low and intermediate values of  $[\text{NADH}]_{\text{av}}$ , we observed period-adding bifurcation sequences (not shown) comparable to those observed at  $\text{pH} \geq 5.2$  when  $[\text{NADH}]_{\text{av}}$  is the bifurcation parameter.<sup>11</sup> At higher NADH levels, the bifurcation scenario changes, and fewer dynamical states are observed. An example is shown in Fig. 3 which displays time series of compound III (coIII). Here, the mean concentration of NADH was maintained at 100  $\mu\text{M}$ , and the concentration of

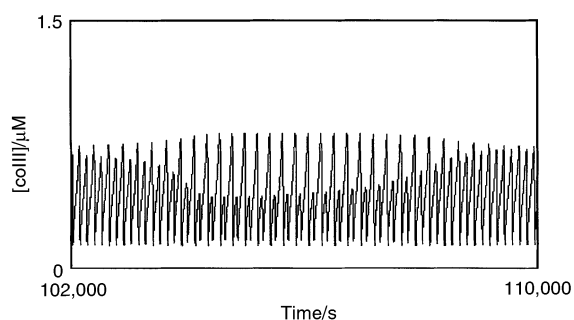


**Fig. 1** Secondary quasiperiodicity as predicted by a detailed model of the PO reaction. Concentrations of the enzyme intermediate, compound III (coIII), evidence period-2 oscillations modulated by an incommensurate frequency. The rate of NADH input,  $\text{NI} = k_{12}[\text{NADH}]_{\text{stock}} = 1.2 \times 10^{-7} \text{ M s}^{-1}$ , the oxygen influx rate,  $k_{13}[\text{O}_2]_{\text{eq}} = 7.2 \times 10^{-8} \text{ M s}^{-1}$  and the oxygen transfer constant,  $k_{-13} = 6 \times 10^{-3} \text{ s}^{-1}$ . Other parameter values as in Table 1 with the following exceptions:  $k_7 = 2 \times 10^7 \text{ M}^{-1} \text{ s}^{-1}$ ,  $k_8 = 9 \times 10^7 \text{ M}^{-1}$

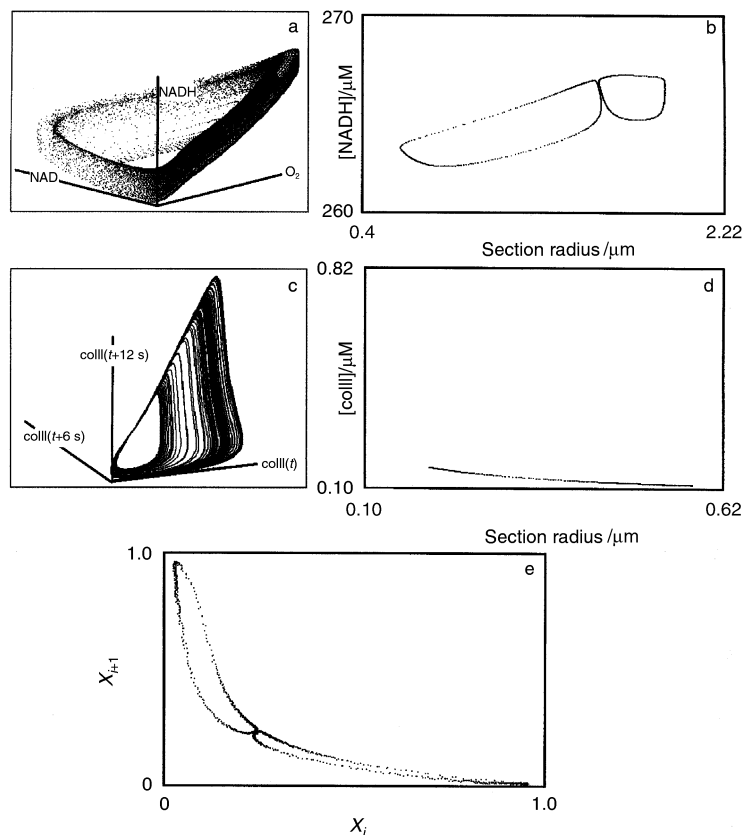


**Fig. 2** Phase space representations of the data in Fig. 1. (a) Asymptotic dynamics projected onto  $[O_2]$ – $[NAD^+]$ – $[NADH]$  space. (b) Poincaré section obtained from the projected phase portrait. (c) Reconstructed trajectory obtained by embedding the time series of  $coIII$  in three dimensions with a time delay of 6 simulated s. (d) Poincaré section obtained from the reconstruction. (e) Return map computed from the Poincaré section in (d) normalized on the interval  $[0,1]$ . Note that while the Poincaré section of the *projected* phase portrait evidences toroidal flow, the section of the *reconstructed* phase portrait is compressed to the point that it is indistinguishable from a one-dimensional curve. In this case, one must look to the return map for evidence of torus dynamics. Compare (c), (d) and (e) with experimental results in Fig. 5.

HBA increased from 230 to 345  $\mu M$ . As the concentration of HBA is increased, the dynamics change from large-amplitude period one ( $1^0$ ) oscillations to large amplitude period-2 ( $1^1$ ) cycles and then to small-amplitude period one ( $0^1$ ) oscillations. Finally, a steady state is observed. In other words, the data suggest simple period bubbling.<sup>12</sup> In these experiments, no other types of dynamics were observed.

#### High oxygen transfer constant experiments

Data from a similar series of experiments (also with  $[NADH]_{av} = 100 \mu M$ ) performed at the high oxygen transfer constant are shown in Fig. 4. Once again, the overall pattern is one of period bubbling. In this case, however, we note a striking deviation: namely, the existence of quasiperiodicity (Fig. 4c) at concentrations of HBA between those corresponding to large amplitude period-2 ( $1^1$ ) cycles and the small-amplitude period-1 ( $0^1$ ) cycles preceding the steady state.

The quasiperiodic time series in Fig. 4c turns out to be “secondary” quasiperiodicity,<sup>18</sup> so-called because the dynamical state subject to incommensurate frequency modulation is a period-doubled (in this case, period-2) cycle. Evidence for this assertion is summarized in Fig. 5. Here, we show a phase plot reconstruction obtained from the time series of  $coIII$  concentrations in Fig. 4c, a Poincaré section and a return map computed from the section. The phase portrait was constructed using Takens’ method of delays<sup>19</sup> with a lag of 6 s. As evidenced by the Poincaré section, the phase plot projection is very thin, with the consequence that its toroidal structure cannot be discerned directly. As in the simulation discussed above, the underlying geometry is revealed by computing the return map (Fig. 5c) which takes the form of paired invariant

loops which are nearly (or actually!) overlapping. In other words, the data suggest Q2 near a fat torus bifurcation as discussed above. An essentially equivalent picture is obtained if one constructs 3-dimensional phase portrait projections (not shown) using the concentrations of ferric peroxidase ( $Per^{3+}$ ), compound III ( $coIII$ ) and dissolved oxygen. Like the reconstructed phase plot in Fig. 4 and, as predicted by the BFSO model, the projections were also very thin. They were also noisier due to noise from the oxygen electrode.

In simulation (see below), the range of parameter values corresponding to secondary quasiperiodicity is quite narrow. This also appears to be the case experimentally, as indicated by the fact that only 20–30% of all experiments conducted at HBA concentrations corresponding to Fig. 4c evidenced quasiperiodic behavior.

## 4. Theoretical

### Methods

The reactions in Table 1 were translated into differential equations which were integrated numerically using a double precision implementation (LSODE) of Gear’s method<sup>22</sup> for solving stiff systems of differential equations. Following a transient of no less than 40 000 simulated seconds, asymptotic dynamics for representative parameter values were computed by accumulating points at time intervals of 1 simulated second. In addition, next amplitude maps were constructed by accumulating 200 000 successive maxima (refined to an accuracy of at least 0.005  $\mu M$ ) in simulated concentrations of  $coIII$ .

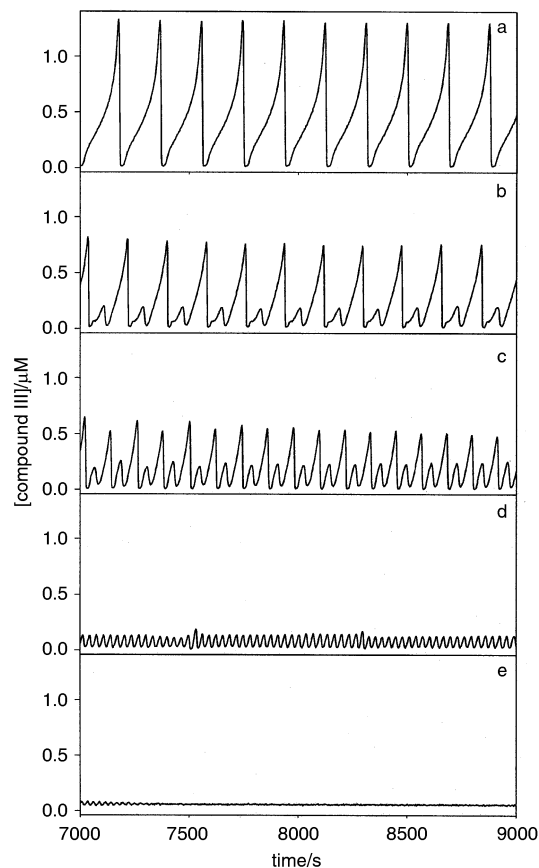


**Fig. 3** Experimental observation of period-bubbling in the peroxidase-oxidase reaction at the low oxygen transfer constant. The concentration of compound III is plotted against time for different concentrations of 4-hydroxybenzoic acid in the reaction mixture: (a) 230; (b) 255; (c) 285; (d) 315  $\mu\text{M}$  and (e) 345  $\mu\text{M}$ . Other conditions as listed in the Experimental section.

Bifurcation diagrams were constructed by accumulating for each of  $450^+$  values of a control parameter, a minimum of 150 successive maxima in simulated concentrations of coIII following a transient of 40 000–100 000 simulated seconds. The diagrams were computed in two ways: (1) the usual one<sup>11,15,18</sup> and (2) so as to mimic the experimental protocol in which  $[\text{NADH}]_{\text{av}}$  was “clamped” to a predetermined value ( $\pm 2\%$ ) by varying the rate of NADH input,  $\text{NI} = k_{12}[\text{NADH}]_{\text{stock}}$ . To simulate changing concentrations of HBA, the principal bifurcation parameter, the rate constant,  $k_8$ , was varied over an appropriate interval. In other words,  $k_8$  was used as a proxy variable for the concentration of aromatic cofactor.<sup>14,17</sup> Unless otherwise noted, the remaining parameter values were as given in Table 1.

## Results

The reconstruction in Fig. 2 bears a striking overall resemblance to the experimental data in Fig. 5. Especially impressive is the similarity of the return maps wherein the inner loops of the torus are close to overlapping. Unfortunately, the details are all wrong. Thus, both the mean concentration of NADH and the maximum concentration of coIII are too high, the former being 265  $\mu\text{M}$  (as opposed to 100  $\mu\text{M}$ ) and the latter, about 1.0  $\mu\text{M}$  (as opposed to about 0.2  $\mu\text{M}$ ). Moreover, the rate constant,  $k_9$ , for NAD radical dimerization, in the simulation was set to  $1.1 \times 10^8 \text{ M}^{-1}\text{s}^{-1}$ , which value, according to the argument of Hauser *et al.*<sup>11</sup> corresponds to pH values below 5.2. In addition, the oxygen transfer constant,  $k_{-13} = 6.0 \times 10^{-3} \text{ s}^{-1}$ , was higher than the experimental value. Most importantly, the quasiperiodic state in simulation is

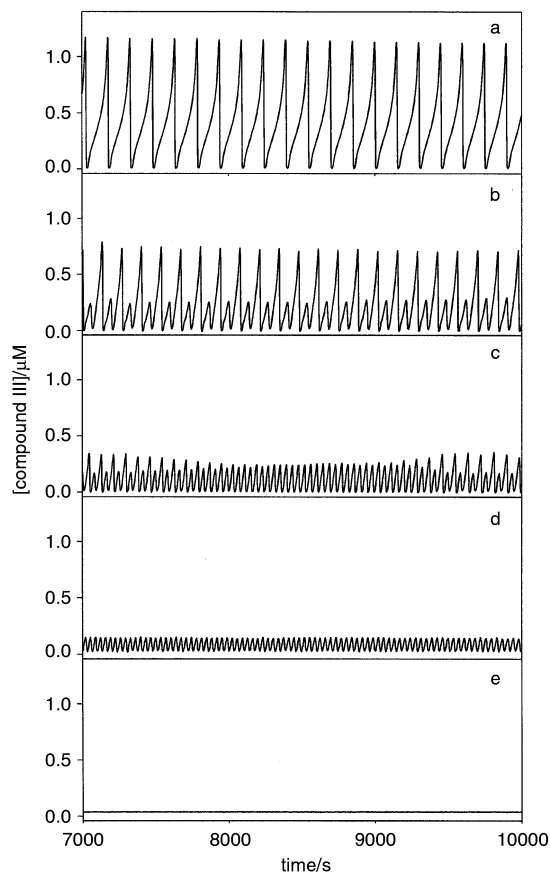


**Fig. 4** Experimental observation of transition to secondary quasiperiodicity at the high oxygen transfer constant. The concentration of compound III is plotted against time for different concentrations of 4-hydroxybenzoic acid in the reaction mixture: (a) 260; (b) 300; (c) 380; (d) 400 and (e) 440  $\mu\text{M}$ . Other conditions as listed in the Experimental section.

situated *between* the  $1^0$  and  $1^1$  cycles as  $k_8$  is increased, whereas in the experiments, Q2 *follows* the  $1^1$  state when the corresponding concentration of HBA is increased.

What happens if we adjust  $[\text{NADH}]_{\text{av}}$ ,  $k_9$  and  $k_{-13}$  to values more appropriate to the experiments reported in Figs. 3 and 4? The answer to this question is shown in Fig. 6. Here we display bifurcation diagrams for which  $k_9 = 6.0 \times 10^7 \text{ M}^{-1} \text{ s}^{-1}$ , which is close to the value ( $5.6 \times 10^7 \text{ M}^{-1} \text{ s}^{-1}$ ) reported by Land and Swallow<sup>23</sup> at pH 6.4, and  $[\text{NADH}]_{\text{av}} = 95.5 \pm 1.9 \mu\text{M}$ , which is close to the experimental set point. The two diagrams correspond to oxygen transfer constants of  $4.7 \times 10^{-3} \text{ s}^{-1}$  (the experimental low value) to  $5.7 \times 10^{-3} \text{ s}^{-1}$  (the experimental high value).

Overall, the two diagrams are quite similar. For the low value of  $k_{-13}$ ,  $1^0$  cycles are succeeded by  $1^1$  oscillations which, in turn, give way to small amplitude, period-1 ( $0^1$ ) cycles. Additionally, there is a region of  $1^2$  cycles (which were not observed experimentally) and a narrow region of more complicated dynamics preceding the onset of small amplitude cycling. For the high value of  $k_{-13}$ , the picture is much the same save that the  $1^2$  cycles disappear.

Of interest to the present discussion are the complex dynamics preceding the small amplitude oscillations at the right. For  $k_{-13} = 4.7 \times 10^{-3} \text{ s}^{-1}$  (low oxygen transfer constant), these correspond to mixed mode oscillations (Fig. 7a) and chaotic intermittency (Fig. 7b). For  $k_{-13} = 5.7 \times 10^{-3} \text{ s}^{-1}$ , one observes a mildly chaotic state (Fig. 8a) which is clearly derived from secondary quasiperiodicity. By this, we mean that the double torus has undergone “fractalization,” even while retaining its essential geometry. This latter state

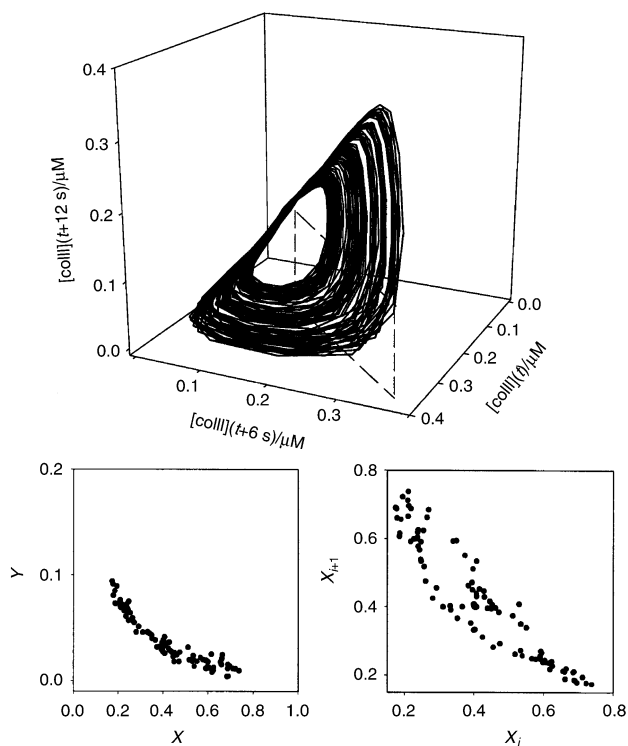


**Fig. 5** Phase plot, Poincaré section and return map of the quasi-periodic oscillations in Fig. 4c. The phase plot in (a) is constructed by lagging the concentration of compound III against itself using a delay of 6 s. The Poincaré section in (b) is constructed by intersecting the flow by the plane indicated in (a). The units on the axis are relative. The return map in (c) is constructed from the X coordinates of the return map in (a).

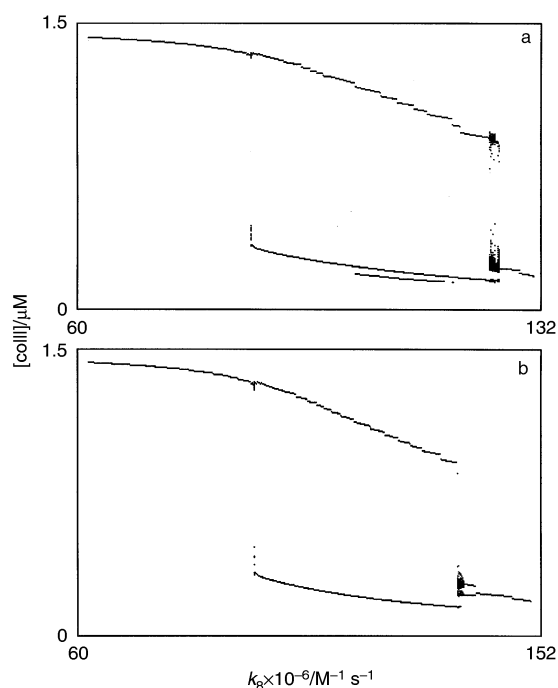


**Fig. 6** Bifurcation diagrams obtained by varying  $k_8$  for low and high values of the oxygen transfer constant,  $k_{-13}$ . (a)  $k_{13}[\text{O}_2]_{\text{eq}} = 5.64 \times 10^{-8} \text{ M s}^{-1}$  and  $k_{-13} = 4.7 \times 10^{-3} \text{ s}^{-1}$ ; (b)  $k_{13}[\text{O}_2]_{\text{eq}} = 6.84 \times 10^{-8} \text{ M s}^{-1}$  and  $k_{-13} = 5.70 \times 10^{-3} \text{ s}^{-1}$ .  $[\text{NADH}]_{\text{av}}$  is fixed at  $95.5 \mu\text{M}$  by varying the rate of NADH input ( $k_{12}$ ). Secondary quasiperiodicity is observed in (b) just prior to the onset of small amplitude period-2 dynamics. Other parameters as in Table 1.

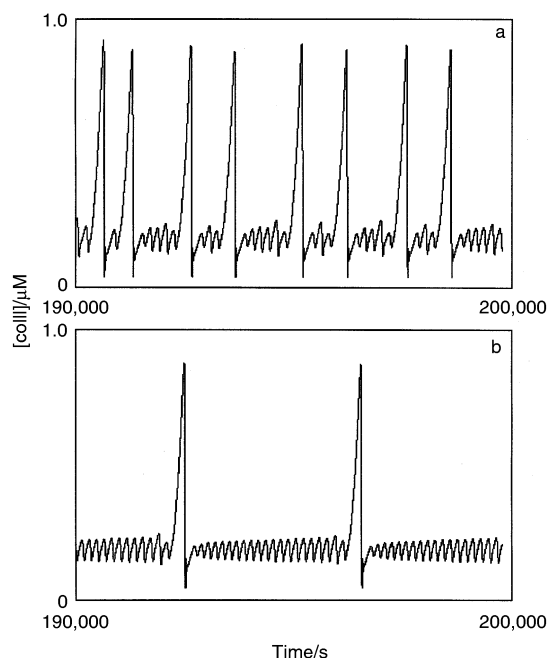


**Fig. 7** Complex dynamics preceding the onset of small amplitude oscillations for  $k_{13}[\text{O}_2]_{\text{eq}} = 5.64 \times 10^{-8} \text{ M s}^{-1}$  and  $k_{-13} = 4.7 \times 10^{-3} \text{ s}^{-1}$  (low oxygen transfer constant). (a) Mixed mode oscillations ( $k_8 = 1.2554 \times 10^8 \text{ M}^{-1} \text{ s}^{-1}$ ;  $\text{NI} = 9.746 \times 10^{-6} \text{ M s}^{-1}$ ). (b) Intermittency ( $k_8 = 1.2648 \times 10^8 \text{ M}^{-1} \text{ s}^{-1}$ ;  $\text{NI} = 1.01835 \times 10^{-7} \text{ M s}^{-1}$ ).

nicely matches the experimental findings in two regards: it occurs at the right place in the bifurcation sequence, and the amplitude of the time series is about right ( $[\text{collIII}] \approx 0.2 \mu\text{M}$ ). On the other hand, the geometry of the attractor, and consequently that of the return map, is wrong. Specifically, the inner margins of the torus, do not approach each other. In short, if the tori in Figs. 2 and 5 are “fat,” the torus in Fig. 8 is “thin.”

## 5. Discussion

### Non-artefactual nature of observed quasiperiodicity

Apparent quasiperiodicity, secondary or otherwise, can result from improper choice of sampling interval. More precisely, sampling the data stream too infrequently can suggest the existence of a second frequency when, in fact, the data are strictly periodic. In the case of the simulations (Figs. 2e and 8f), this is not a problem. The peak sharpening routine used to compute the next amplitude maps, whereby maxima were characterized to an accuracy of  $0.005 \text{ mM}$ , guarantees the reality of the invariant loops. As a check, sample calculations were carried out with the maxima estimated to much greater precision, with no change in the results. In the case of the experimental data, no such option was available. Accordingly, we investigated the consequences of *increasing* the sampling interval, *i.e.* by sub-sampling the data, for experimentally observed period-2 oscillations, the principal frequency of which was close to that of the quasiperiodic state in Fig. 4c. Only after increasing the sampling interval from 2 s (the interval at which the data were actually collected) to more than 10 s, did we observe a change in apparent dynamics to anything remotely resembling quasiperiodicity.

### Theory vs. experiments

On the face of it, the preceding observations would appear to indicate that while BFSO can account for secondary quasiperiodicity at high concentrations of HBA, it is incapable of reproducing the experimentally observed state which is close to

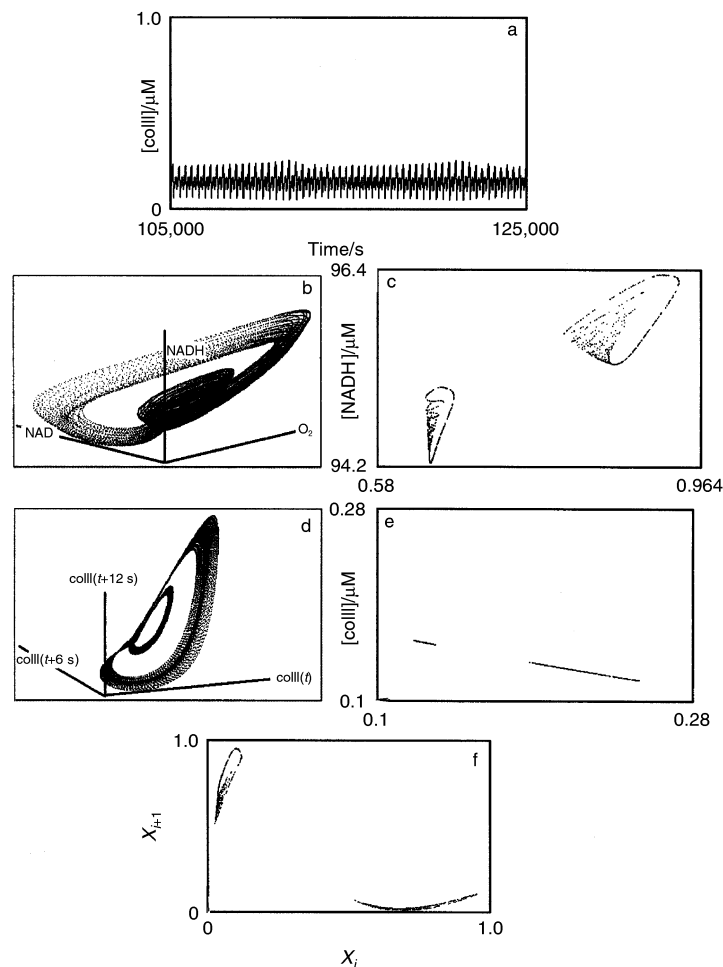


**Fig. 8** Secondary quasiperiodicity preceding the onset of small amplitude cycles for  $k_{13}[\text{O}_2]_{\text{eq}} = 6.84 \times 10^{-8} \text{ M s}^{-1}$  and  $k_{-13} = 5.7 \times 10^{-3} \text{ s}^{-1}$  (high oxygen transfer constant) with  $k_8 = 1.38 \times 10^8 \text{ M}^{-1} \text{ s}^{-1}$  and  $\text{NI} = 1.2371 \times 10^{-7} \text{ M s}^{-1}$ . (a) Time series of coIII. (b) Projected phase portrait. (c) Poincaré section. (d) Reconstructed phase plot computed from the time series using a lag of 6 simulated s. (e) Poincaré section of the reconstruction. (f) Return map computed from the Poincaré section in (e) normalized on the interval [0,1].

a fat torus bifurcation. In fact, fat torus bifurcations at high values of [HBA] are predicted by the model, but they appear only to occur *after* the torus has been destabilized. Still, the double torus persists, but as a chaotic saddle or semiattractor<sup>24</sup> contained within a larger attracting set. The observable consequence is dynamics of the sort shown in Fig. 7b.

In greater detail, one observes the sequence of dynamical states documented in Fig. 9. Here, we display next amplitude maps ( $k_8 = 1.38 \times 10^8 \text{ M}^{-1} \text{ s}^{-1}$ ;  $k_{13} = 5.7 \times 10^{-3} \text{ s}^{-1}$ ) for decreasing rates of NADH input. Starting with  $\text{NI} = 1.23715 \times 10^{-7} \text{ M s}^{-1}$ , we observe a thin double torus (not shown) which thereafter begins to wrinkle. That is, the torus undergoes a homoclinic transition to chaos, a “thin torus” bifurcation, if you will, which leads to the chaotic state shown in Fig. 8. With continuing reductions in NADH input, the homoclinic tangles become more pronounced (Fig. 9a). At this point, what was once a double torus is now a two-piece chaotic attractor. Further reductions in NADH input result in a transition to large amplitude chaos whereby the map acquires two additional pieces (Fig. 9b). Eventually, the remnants of the torus interact with each other and with the stable manifold of the non-stable period-1 cycle between them (Fig. 9c). At this point, there is a fat torus bifurcation as discussed above, but with the difference that the bifurcating set has already been destabilized. Magnification (Fig. 9d) reveals the tangling of torus and manifold. Because the interacting torus and manifold are contained within a larger chaotic attractor, the temporal picture

is one of intermittency: small amplitude oscillations, corresponding to motion in the tangle, punctuated by occasional irruptions. Summarizing, one observes the following sequence:

Thin torus Q2  $\rightarrow$  Thin torus chaos  $\rightarrow$  Large amplitude chaos  
 $\rightarrow$  Intermittency

In short, the essential discrepancy between theory and data, *i.e.* thin tori *vs.* fat, approximate quasiperiodicity *vs.* intermittency, boils down to the fact that in the model, the double torus is destabilized before it has a chance to fatten, whereas the experimental picture suggests no such destabilization. From a chemical perspective, the source of this discrepancy remains problematic. Surely,<sup>25</sup> the BFSO model omits a great deal of chemistry and, as recently reviewed,<sup>17</sup> there remain uncertainties regarding parameter values. With regard to the latter point, it may well be relevant, that in our previous papers, BFSO was “calibrated” for experiments utilizing DCP. As discussed by Hauser and Olsen,<sup>26</sup> different cofactors probably utilize the same mechanism to induce oscillations in the PO reaction. However, different phenolic compounds may induce different types of dynamics, depending on the reduction potential for the formation of the phenoxyl radical. Thus, the substitution of HBA for DCP may have additional consequences not taken into account here. Consistent with this possibility is the fact that next-amplitude maps which are at least superficially similar to

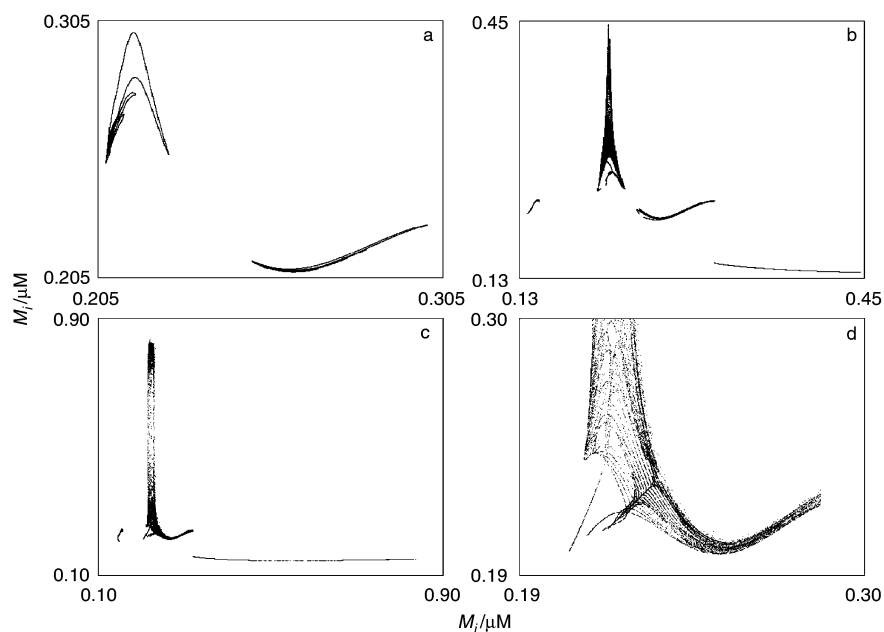


**Fig. 9** Next amplitude maps illustrating the transition from thin torus dynamics to intermittency for  $k_{13}[\text{O}_2]_{\text{eq}} = 6.84 \times 10^{-8} \text{ M s}^{-1}$  and  $k_{-13} = 5.7 \times 10^{-3} \text{ s}^{-1}$  (high oxygen transfer constant) with  $k_8 = 1.38 \times 10^8 \text{ M}^{-1} \text{ s}^{-1}$ . (a)  $\text{NI} = 1.2368 \times 10^{-7} \text{ M s}^{-1}$ . (b)  $\text{NI} = 1.2350 \times 10^{-7} \text{ M s}^{-1}$ . (c)  $\text{NI} = 1.2300 \times 10^{-7} \text{ M s}^{-1}$ . (d) Magnification of (c) showing fat torus tangling of the inner margins of the period-doubled torus and the stable manifold of the period-1 cycle.

those in Fig. 9 have been observed in the course of experiments utilizing DCP (M.J.B. Hauser and L.F. Olsen, unpublished).

In conclusion we offer the following observations:

1. The simulations presented in Fig. 9 suggest a new, “thin torus,” route to chaos involving period-doubled tori.

2. These calculations also indicate that fat torus bifurcations come in two flavors: (i) “simple” FTBs, in which case the bifurcating set is an attractor and (ii) “interior” FTBs, in which case the bifurcating set is a semi-attractor. As noted above, the time series associated with these two scenarios are very different.

3. As previously observed,<sup>18</sup> the existence of toroidal dynamics underscores the essentially two-dimensional character of peroxidase–oxidase dynamics when viewed in section. The implication is that one-dimensional interpretations, for example, in terms of logistic-like return maps, are, at best, approximate.

4. In this regard, the thin torus route provides a mechanism whereby behaviour which is manifestly two-dimensional gives way to dynamics for which a one-dimensional description is an acceptable approximation. At the same time, this scenario suggests that at least some of the “fuzzi-ness” in experimental return maps<sup>13</sup> is real and not artifactual.

5. The experimental confirmation of predictions such as the observation of period-doubled tori and fat torus bifurcations, which are both dynamically delicate and restricted to narrow intervals of parameter values, offers additional evidence for both the resolving power of the experimental technique and the predictive power of the BFSO model.

Altogether, we believe the foregoing results exemplify the way in which mechanistic modelling and careful experimentation can mutually enrich and inform each other. This approach, when it works, is a puissant symbiosis.

## Acknowledgements

This research was supported by grants from the Danish Natural Science Research Council to LFO. The authors thank Anita Lunding for skilled technical assistance.

## References

- 1 S. Nakamura, K. Yokota and I. Yamazaki, *Nature*, 1969, **222**, 794.
- 2 A. Scheeline, D. L. Olson, E. P. Williksen, G. A. Horras, M. L. Klein and R. Larter, *Chem. Rev.*, 1997, **97**, 739.
- 3 H. B. Dunford, *Heme Peroxidases*, Wiley, New York, 1999.
- 4 M. J. B. Hauser and L. F. Olsen, in *Transport and Structure—Their Competitive Roles in Biophysics and Chemistry*, ed. S. C. Müller, J. Parisi and W. Zimmermann, Springer, Berlin, 1999, 252–272.
- 5 B. P. Belousov, *Sb. Ref. Radiat. Med.*, Medgiz, Moscow, 1958, 145.
- 6 A. M. Zhabotinskii, *Biofizika*, 1964, **9**, 306.
- 7 T. Hauck and F. W. Schneider, *J. Phys. Chem.*, 1993, **97**, 391.
- 8 M. S. Samples, Y.-F. Hung and J. Ross, *J. Phys. Chem.*, 1992, **96**, 7338.
- 9 L. F. Olsen and H. Degn, *Nature*, 1977, **267**, 177.
- 10 M. J. B. Hauser and L. F. Olsen, *J. Chem. Soc. Faraday Trans.*, 1996, **92**, 2857.
- 11 M. J. B. Hauser, L. F. Olsen, T. V. Bronnikova and W. M. Schaffer, *J. Phys. Chem. B*, 1997, **101**, 1075.
- 12 M. Bier and C. Bountis, *Phys. Lett. A*, 1984, **104**, 239.
- 13 T. Geest, C. G. Steinmetz, R. Larter and L. F. Olsen, *J. Phys. Chem.*, 1992, **96**, 5678.
- 14 T. V. Bronnikova, V. R. Fed’kina, W. M. Schaffer and L. F. Olsen, *J. Phys. Chem.*, 1995, **99**, 9309.
- 15 T. V. Bronnikova, W. M. Schaffer, M. J. B. Hauser and L. F. Olsen, *J. Phys. Chem. B*, 1998, **102**, 632.
- 16 T. V. Bronnikova, W. M. Schaffer and L. F. Olsen, *J. Phys. Chem. B*, 2001, **105**, 310.
- 17 T. V. Bronnikova, W. M. Schaffer and L. F. Olsen, *J. Chem. Phys.*, 1996, **105**, 10 849.
- 18 F. Takens in *Dynamical Systems and Turbulence* ed. D. Rand and L.-S. Young, Springer, Berlin, 1981, 366.
- 19 J.-C. Roux, R. H. Simoyi and H. L. Swinney, *Physica D*, 1983, **8**, 395.
- 20 M. J. B. Hauser, A. Lunding and L. F. Olsen, *Phys. Chem. Chem. Phys.*, 2000, **2**, 1685.
- 21 A. C. Hindmarsh, *ACM Signum Newsletter*, 1980, **15**, 10.
- 22 E. J. Land and A. J. Swallow, *Biochim. Biophys. Acta*, 1968, **162**, 327.
- 23 H. Kantz and P. Grassberger, *Physica D*, 1985, **17**, 75.
- 24 E. S. Kirkor and A. Scheeline, *Eur. J. Biochem.*, 2000, **267**, 5014.
- 25 M. J. B. Hauser and L. F. Olsen, *Biochemistry*, 1998, **37**, 2458.